Delft University of Technology

FACULTY OF CIVIL ENGINEERING AND GEOSCIENCES
Track of Structural Engineering

Report on
"The dynamic response of an embedded cavity in a half-space subjected to SH waves using the Boundary Element Method"

Author: Jun Yuan
Date: 8-Dec-2017

Report on
“The dynamic response of an embedded cavity in a half-space subjected to SH waves using the Boundary Element Method”

Author: Jun Yuan

Supervisor:
Karel van Dalen
Mingjuan Zhao
Apostolos Tsouvalas

Faculty of Civil Engineering and Geoscience
Section of Structural Mechanics
Research Group of Structural Dynamics

Acknowledgements

This additional thesis was written as part of the Civil Engineering curriculum (10 ECTS) at the Delft University of Technology, for the master track of Structural Engineering.

This research started from mid May and was completed in November with summer vacation in between, of course. I spent time more than expected because I was working part time and I wish to focus more dedicatedly on my coming final thesis.

I would like to express my appreciation to all those who contributed in the fulfillment of my additional thesis work. Firstly, I would like to thank Karel, for giving me this opportunity and give valuable feedback when I encountered problems or things that I could not explain. His opinion is always helpful and to the point. Secondly and most importantly, I would like to thank Mingjuan, my 'weekly' supervisor. I would not use the word 'daily supervisor' because if I have visited her office and asked her problems everyday then she probably would have been annoyed. Anyways, Mingjuan did teach me a lot and she is always patient to explain everything. Thank you all for your time and your guidance.

J.(Jun) YUAN
Delft, December 2017

Abstract

A reciprocity-based direct boundary integral method and indirect boundary integral method have been introduced and used to obtain the two-dimensional response of a cylindrical cavity embedded in a uniform elastic half space subjected to SH wave. By introducing free wave field and the actual field with a cavity, the key point to solve for scattered wave field is cavity boundary integral. In order to do so, plane waves generated by free wave field and a 2D Green's function for a half space are used. To overcome the limitations of direct boundary integral method, an indirect boundary integral method provided by a classical case study is used. In the end, results are calculated by the latter method, indirect boundary method, and are used to compare with the results from the classical case study.

Contents

1. PROBLEM STATEMENT

The rapid development of underground railway lines brings passengers great convenience, meanwhile, also the concern of safety. The waves excited by earthquakes can destabilize the operation of underground railway system, where horizontally polarized shear wave plays a dominant role in causing damages to structures. Therefore, it is of great importance to study the dynamic response of the railway tunnels subjected to SH wave excitation during earthquakes.

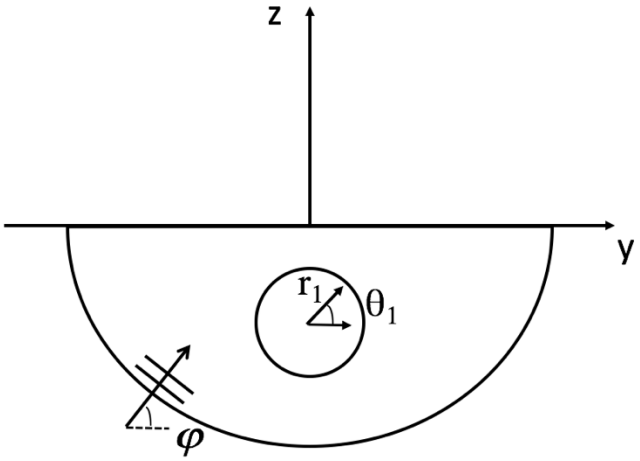

Figure 1.1 A half-space model

Consider a half-space model consisting of linear elastic homogeneous soil and a cavity as depicted in Figure 1.1, yz-plane is the vertical plane representing a cross section of earth. When a horizontally polarized shear wave propagates from below towards the tunnel, the particle motion in the x-direction (horizontal direction) is of prime concern, which makes the particle motion in the vertical direction trivial, that is

$$u_y = 0, \ \ u_z = 0 \tag{1.1}$$

Also, consider the wave in the horizontal direction homogenous, which gives

$$\frac{\partial}{\partial x} = 0 \tag{1.2}$$

The equation of motion for linear elastic homogeneous continuum can be referred to the Lecture Note of *CIE5340 Soil Dynamics[1]*. The equation of equilibrium can be reached by considering a small element, and it can be written in the full index notation

$$\sigma_{ij,j} = \rho \ddot{u}_i \tag{1.3}$$

The full constitutive equation for the linear elastic 3D model using the index notation can be described as:

$$\sigma_{ij} = \lambda \varepsilon_{kk} \delta_{ij} + 2G\varepsilon_{ij} \tag{1.4}$$

where δ_{ij} is the Kronecker operator defined by:

$$\delta_{ij} = \begin{cases} 1 & \text{if i = j} \\ 0 & \text{if i} \neq \text{j} \end{cases} \tag{1.5}$$

The kinetic equation gives the relation between displacement and strain,

$$\varepsilon_{ij} = \frac{1}{2}(u_{i,j} + u_{j,i}) \tag{1.6}$$

Finally, substituting equation of Eq(1.4) and Eq(1.6) into Eq(1.3), the equation of motion for the the elastic continuum is found

$$\rho \ddot{u}_i = \lambda u_{k,ki} + G(u_{i,jj} + u_{j,ij}) \tag{1.7}$$

where λ and G are the well-known Lamé constants, the latter also known as the shear modulus. K is the bulk modulus and ρ the density. They have the following relation

$$\lambda = K - \frac{2}{3}G \tag{1.8}$$

Taking the characteristics of the problem Eq(1.1) and Eq(1.2) into account, relevant terms in Eq(1.7) are reduced, which gives the equation of motion only in the x direction

$$\rho \ddot{u}_x - G\nabla^2 u_x = 0 \tag{1.9}$$

Here, only $u_x(t,y,z)$ is unknown, therefore the vector problem is transformed into a scalar problem. In case, the Laplace operator ∇^2 in the Cartesian coordinate represents

$$\nabla^2 = \frac{\partial^2}{\partial y^2} + \frac{\partial^2}{\partial z^2} \tag{1.10}$$

We recognize Eq(1.9) a 2D wave equation for SH wave in linear elastic homogeneous continuum, which incorporates a second order time derivative and a second order spatial partial derivative. To solve the partial differential equation, we apply the Fourier transform over time

$$U_x(\omega,y,z) = \int_{-\infty}^{+\infty} u_x(t,y,z) e^{-i\omega t}\, dt \tag{1.11}$$

Note that by using Fourier transform, initial conditions are required to be zero. Similarly, apply Fourier transform to equation of motion Eq(1.9), we obtain

$$\rho(i\omega)^2 U_x - G\nabla^2 U_x = 0$$

or

$$\nabla^2 U_x + k_s^2 U_x = 0 \tag{1.12}$$

where $k_s = \omega / c_s$ is the wave number, $c_s = \sqrt{G/\rho}$ the shear wave speed. This is the governing equation of motion in the frequency domain. If we look at the equation of motion Eq(1.9) in the time domain, since it is second derivative with respect to time, second derivative with respect to *y* and second derivative with respect to *z,* normally we would need 2 boundary conditions with respect to *y* and 2 boundary conditions with respect to *z.* Moreover, we need 2 initial conditions with respect to time, i.e, being the initial displacement and initial velocity. However, here we impose zero initial conditions for the problem and only based on this, one can perform the Fourier transform.

The equation of motion can be solved in the free wave field case (will be discussed in the next section) where there is no such a cavity, from which a plane wave solution will be obtained. However, with the presence of the cavity, Eq(1.9) has to satisfy boundary conditions both at the free surface *z=0* and at cavity surface $r=r_0$ due to the fact that they are traction-free surface, which are

$$z = 0,\ \sigma_{zx} = 0 \tag{1.13}$$

and

$$r_1 = r_0,\ \sigma_{r_1 x} = 0 \tag{1.14}$$

They are the two intuitive boundary conditions that are imposed to describe the field wave. Eq(1.13)describes the dynamic boundary condition with respect to z ,and Eq(1.14) describes the dynamic boundary condition with respect to *y* and *z*. (in the polar coordinate). It is worth noticing that there is another intrinsic boundary condition that is left imposed on the system, which is the radiation condition. At infinite distance away from *z=0,* the displacement is set to be zero.

$$z \to -\infty \text{ or } |y| \to \infty, u_x < \infty \tag{1.15}$$

It should be noted that these boundary conditions are defined under different coordinates, therefore, it's possible but very difficult to impose them into just one equation of motion.

In this paper, direct boundary integral method and indirect boundary integral method, will be introduced to solve the problem. It will be further discussed in the next chapter.

2. METHOD OF SOLUTION

2.1 Reciprocity Theorem

The main idea of reciprocity is that two admissible elastodynamic states can be associated with its own set of time-invariant parameters and its own set of loading conditions.[2] The starting point for the reciprocity is the equations of equilibrium for two states A and B,

$$\tau_{ij,i}^{A} + f_j^{A} = \rho \ddot{u}_j^{A} \tag{2.1}$$

$$\tau_{ij,i}^{B} + f_j^{B} = \rho \ddot{u}_j^{B} \tag{2.2}$$

The first and the second equation are multiplied by u_j^B and u_j^A, respectively. Subtraction of the second equation from the first one, using integration by parts and the Hooke's law, the expression can be written as

$$(f_j^A - \rho \ddot{u}_j^A)u_j^B - (f_j^B - \rho \ddot{u}_j^B)u_j^A = -(\tau_{ij,i}^A u_j^B - \tau_{ij,i}^B u_j^A) = (\tau_{ij}^B u_j^A - \tau_{ij}^A u_j^B)_{,i} \tag{2.3}$$

Considering terms as time-harmonic related, we can integrate the expression over a volume $\boldsymbol{V}$ with boundary $\boldsymbol{S}$, and then apply Gauss' theorem to convert the right-hand side into a surface integral, therefore Eq (2.3) yields

$$\int_V (f_j^A u_j^B - f_j^B u_j^A) dV = \int_S (\tau_{ij}^B u_j^A - \tau_{ij}^A u_j^B) n_i dS \tag{2.4}$$

where $\boldsymbol{n}$ is the unit vector along the outward normal to $\boldsymbol{S}$. The terms in the integral are now dependent only on position because they are considered to be time-harmonic. This is the global reciprocity theorem which connects state A and state B. More detailed derivations can be referred to literature [2].

2.2 Direct Boundary Integral Method

Based on the reciprocity theorem, direct boundary integral equation is obtained by implementing the terms in Eq(2.4) in a more specific way. Here, we consider the whole soil continuum as the integration region $\boldsymbol{V}$ (shadow part shown in Figure 2.1), and the cavity surface $r_1 = r_0$ as the boundary $\boldsymbol{S}$ (cavity surface solid line). State A represents the green function state, and state B represents the unknown half-space with cavity. The Green's function state A is the full half-space which is considered known. It is a function with regard to time and spatial coordinate. It describes the dynamic characteristic behavior of the system and it depends only on the system itself.

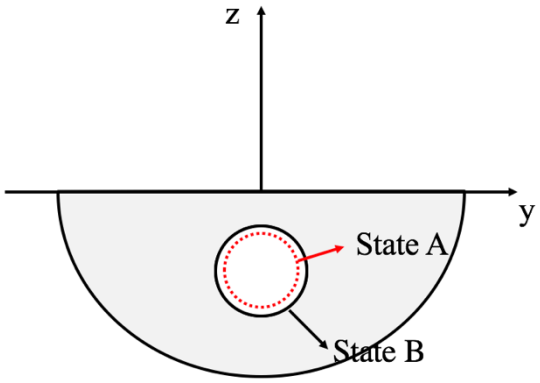

Figure 2.1 A half-space model with two states

Here, we choose excitation sources located very close to the inner surface of the boundary, therefore, the body force f_j^A can be considered outside the integration region V and does not contribute in the integral. It is a non-zero value but exists in the reference system, therefore, it does not contribute in the boundary integral. On the other hand, state B can be regarded as the response state in the soil and there is no body force in the soil, which directly gives zero value.

$$f_j^A = 0\,, \quad f_j^B = 0 \tag{2.5}$$

Combining both, we can conclude that: the left hand side of the integral equation is equal to zero, Eq(2.4) yields

$$\int_S (\tau_{ij}^B u_j^A - \tau_{ij}^A u_j^B) n_i dS = 0 \tag{2.6}$$

The response state B is the scattered wave field which is generated from the cavity surface. In the end, the reciprocity theorem for boundary integral method can be expressed as

$$\int_S [\sigma_{r_1 x}^{sc}(\underline{x}) u_x^*(\underline{x},\underline{x}_0) - \sigma_{r_1 x}^*(\underline{x},\underline{x}_0) u_x^{sc}(\underline{x})] dS = 0 \tag{2.7}$$

where $u_x^*(\underline{x},\underline{x}_0) = u_x^*(y,z;y_0,z_0)$ is the displacement field represented by green function state A. It is a function of the response position and the excitation source position. Any arbitrary loadings can be expressed in the form of green function, but with amplification factor and a shift of the position (or time). In case, it satisfies the following equation of motion, which is from Eq(1.8) but now with a right hand side. Now it yields

$$\nabla^2 u_x^* + k_s^2 u_x^* = \frac{1}{G}\delta(y-y_0)\delta(z-z_0) \tag{2.8}$$

Furthermore, in practice, the discretized form of boundary integral may be expressed as follows, where $(\underline{x}_i,\underline{x}_{0,j})$ means the response at location (y_i,z_i) due to the impulse excitation at location $(y_{0,j},z_{0,j})$. For every source point, one can obtain the following

$$\sum_{i=1}^{N_O} [\sigma_{r_1 x}^{sc}(\underline{x}_i) u_x^*(\underline{x}_i,\underline{x}_{0,j}) - \sigma_{r_1 x}^*(\underline{x}_i,\underline{x}_{0,j}) u_x^{sc}(\underline{x}_i)] = 0 \tag{2.9}$$

Integration over boundary line S represents the summation over receiver locations in the discretized form of representation. Superscript * means the green function and superscript '*sc*' stands for unknown scattered fields. Green function state A is known

here, while stress field is nothing more than a first derivative of displacement with regard to r_1. What's more, the unknown shear stress from the scattered field can be written by shear stress in the free wave field but with a minus sign because of the boundary condition that it has to fulfill. Therefore, this summation contains N unknown scattered displacement components. To solve these N unknowns, one needs N equations which can be done by considering impulse excitations at N different positions.

2.3 Free Wave Field

We identify two systems which needs to be considered. The first one is the free field system without a cavity as a reference system, and the second one is the actual system with a cavity placed.

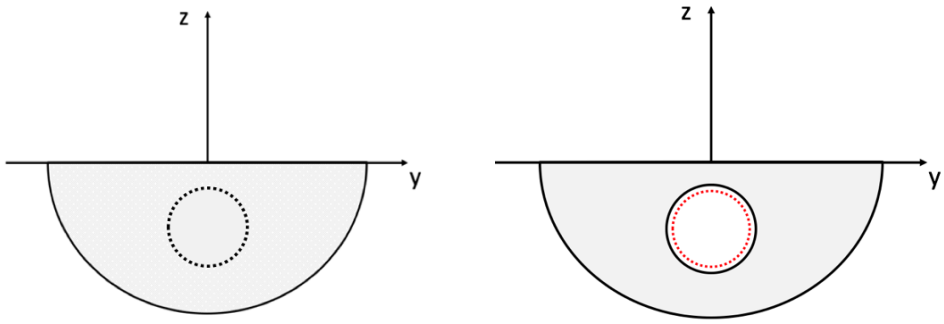

(a)Reference system *(b)Actual system*

Figure 2.2 (a)reference system and (b)actual system

The free field is composed of incident and reflected waves. For the free field system, the response is already solved due to the existence of the green function. Using the green function, the response in the frequency domain is nothing more than a multiplication of this transfer function and the Fourier transform of the external force. In a special case where the excitation is the impulse excitation, the frequency response of the system is simply the green function itself, which is the case that we consider.

For the actual system, the existence of the cavity will disturb the free field. Apart from incident wave and reflected wave which are included in the free wave field, another type of wave will be introduced -scattered wave. Therefore, the actual field is a total field of free wave field and scatter wave field. [3]

$$u_x^{tot} = u_x^{free} + u_x^{sc} \tag{2.10}$$

Similarly, the total stress field is the sum of free stress field and scattered stress field.

$$\sigma_{r_1 x}^{tot} = \sigma_{r_1 x}^{free} + \sigma_{r_1 x}^{sc} \tag{2.11}$$

For the actual system, the zero traction-free condition holds at the cavity surface, as already depicted in Eq(1.14). It can be seen as a summation of shear stress in the scattered field around the cavity and shear stress in the free field at exactly the same locations. Although the two systems have different response outside the cavity area, they have an overlapped cavity boundary. And the total stress on this boundary caused by the free field and scattered field is essentially zero. This is the link of the two systems

and we can make use of it, in the end, replacing the scattered stress term by the free stress term, but with a minus sign.

$$r_1 = r_0,\ \sigma_{r_1 x}^{sc} = -\sigma_{r_1 x}^{free} \tag{2.12}$$

Furthermore, the scattered stress term in boundary integral Eq(2.7) can be replaced. The equation of motion that governs the free vibration of soil subjected to SH wave is given as Eq(1.12), the general solution to the differential equation could be expressed in exponential form

$$U_x^{inc}\ (\omega, y, z) = U_1 \exp(-ik_y y - ik_z z + i\omega t) \tag{2.13}$$

This is the incident wave field. But substituting this solution into equation of motion Eq(1.12), the following dispersion equations are obtained

$$[(ik_y)^2 + (ik_z)^2)]\exp(-ik_y y - ik_z z) - k_s^2 \exp(-ik_y y - ik_z z) = 0 \tag{2.14}$$

Or in a simplified form,

$$k_y^2 + k_z^2 = k_s^2 \tag{2.15}$$

where $k_s = \omega / c_s$ is the wave number in the main direction, k_y and k_z are the component of wave number in the y and z direction, respectively. φ is the angle between the direction of wave number k_s and y axis, shown in Figure 2.1.

$$k_y = k_s \cdot \cos\varphi,\ k_z = k_s \cdot \sin\varphi \tag{2.16}$$

Likewise, the outgoing wave is reflected back from the upper free surface, with the direction which is towards the negative *z* direction. The sign in the expression indicates the direction, therefore, the total wave is a summation of an incident wave (in the positive y and z direction) and a reflected wave from the upper free boundary (in the positive y and negative z direction).

$$U_x(\omega, y, z) = U_1 \exp(-ik_y y - ik_z z) + U_2 \exp(-ik_y y + ik_z z) \tag{2.17}$$

Substituting the general solution onto the boundary condition at *z = 0*, one obtains that the coefficients in the two terms are equal. Therefore, the free wave field could be simplified

$$U_x(\omega, y, z) = U_0 \cdot [\exp(-ik_y y - ik_z z) + \exp(-ik_y y + ik_z z)] \tag{2.18}$$

Furthermore, stress field in the frequency domain can be calculated by taking the first derivative of displacement. Here, the stress involves a conversion from cylindrical coordinate to Cartesian coordinate.

$$\sigma_{r_1 x}^{free}(\omega, y, z) = G \frac{\partial U_x}{\partial r_1} \tag{2.19}$$

Note that the derivative of U_x is with regard to r_1 which is the local coordinate of the cavity, but the displacement was defined in the global coordinate (which is originated on the ground surface.) Therefore, the transformation between the global and local coordinates are as follows, superscript '$_1$' denotes the local coordinate at the cavity

$$\begin{cases} y = y_1 \\ z = z_1 - H \end{cases} \tag{2.20}$$

Rewrite the displacement in the local Cartesian coordinate

$$U_x(\omega, y, z) = U_1 \cdot [\exp(-ik_y y_1 - ik_z (z_1 - H)) + \exp(-ik_y y_1 + ik_z (z_1 - H))] \tag{2.21}$$

Cartesian coordinate can be further expressed in cylindrical coordinate θ_1 and r_1.

$$\begin{cases} y_1 = r_1 \cdot \cos\theta_1 \\ z_1 = r_1 \cdot \sin\theta_1 \end{cases} \tag{2.22}$$

In the end, the displacement in terms of local cylindrical coordinate can be expressed as:

$$U_x(\omega, y, z) = U_1 \cdot [\exp(-ik_y r_1 \cos\theta_1 - ik_z(r_1 \sin\theta_1 - H)) + \exp(-ik_y r_1 \cos\theta_1 + ik_z(r_1 \sin\theta_1 - H))] \tag{2.23}$$

The shear stress $\sigma_{r_1 x}^{free}$ is written as:

$$\begin{aligned} \sigma_{r_1 x}^{free}(\omega, y, z) = {} & GU_0(-ik_y \cos\theta_1 - ik_z \sin\theta_1)[\exp(-ik_y r_1 \cos\theta_1 - ik_z(r_1 \sin\theta_1 - H))] \\ & + GU_0(-ik_y \cos\theta_1 + ik_z \sin\theta_1)[\exp(-ik_y r_1 \cos\theta_1 + ik_z(r_1 \sin\theta_1 - H))] \end{aligned} \tag{2.24}$$

It can also be written as:

$$\begin{aligned} \sigma_{r_1 x}^{free}(\omega, y, z) = {} & GU_0(-ik_y \cos\theta_1 - ik_z \sin\theta_1)[\exp(-ik_y y - ik_z z)] \\ & + GU_0(-ik_y \cos\theta_1 + ik_z \sin\theta_1)[\exp(-ik_y y + ik_z z)] \end{aligned} \tag{2.25}$$

Therefore, shear stress $\sigma_{\theta_1 x}$ is shown:

$$\begin{aligned} \sigma_{\theta_1 x}^{free} = {} & GU_0(+ik_y r_1 \sin\theta_1 - ik_z r_1 \cos\theta_1)\exp(-ik_y y - ik_z z) \\ & + GU_0(ik_y r_1 \sin\theta_1 + ik_z r_1 \cos\theta_1)\exp(-ik_y y + ik_z z) \end{aligned} \tag{2.26}$$

So far, the free field has been solved and the shear stress term $\sigma_{r_1 x}^{sc}$ in the boundary integral is represented by $\sigma_{r_1 x}^{free}$. In the next section, more insight into the green function will be investigated. The shear stresses are important to know, since $\sigma_{r_1 x}^{tot}$ can be checked whether it is equal to zero in order to satisfy the boundary condition around the cavity surface, and $\sigma_{\theta_1 x}^{free}$ is essentially non zero value in this case.

2.4 Green's Function(2D) of a Half-space

Green's function, referred as frequency response function (FRF) or transfer function, describes the dynamic behavior of a system can be used to calculate the response under a known excitation. Take a single-degree-of-freedom system as an example,

$$m\ddot{u}(t) + c\dot{u}(t) + ku(t) = F(t) \tag{2.27}$$

we apply Fourier transform of the equation of motion of a mass-spring system, the response in the frequency domain is derived.

$$U(\omega) = \frac{F(\omega)}{-\omega^2 m + i\omega c + k} \tag{2.28}$$

Consider an impulse excitation represented by a Dirac-delta function, its Fourier transform gives a unit amplitude, moreover, if there is no time shift in the function, the impulse response happens to be equal to the green function, which is:

$$G(\omega)=\frac{1}{-\omega^2 m+i\omega c+k} \tag{2.29}$$

By applying inverse Fourier transform of the green function, one obtains the displacement response back in the time domain.

Similarly, for a 2D half-space subjected to an impulsive line load, the governing equation of motion has been given in Eq(2.8) in the frequency domain. Furthermore, Fourier transform is performed with regard to spatial coordinate y and z (Here, we discuss firstly the Green's function for infinitely large full space). The Fourier transform over time *t* and space, y and z, are defined as:

$$\tilde{\tilde{u}}^*(\omega,k_y,k_z)=\int_t\int_y\int_z u(t,y,z)\cdot e^{i\omega t-ik_y y-ik_z z}dzdydt \tag{2.30}$$

For a simple case where an impulse excitation with unit amplitude, which is located in the origin *(0,0)*, one obtains the 2D green function:

$$\tilde{\tilde{u}}^*(\omega,k_y,k_z)=\frac{1}{k_s^2-k_y^2-k_z^2} \tag{2.31}$$

Normally, apply double inverse Fourier transforms over wave number k_y and k_z, the response back in the frequency-space domain can be obtained:

$$u^*(\omega,y,z)=\frac{1}{4\pi}\int_{-\infty}^{+\infty}\int_{-\infty}^{+\infty}\frac{1}{k_s^2-k_y^2-k_z^2}\cdot e^{+ik_y y+ik_z z}dk_y dk_z \tag{2.32}$$

However, this partial differential equation is difficult to be integrated in the Cartesian coordinate. Therefore, this problem is tackled by transforming Cartesian coordinate to the cylindrical coordinate. Here, $y=r\cdot\cos\theta, z=r\cdot\sin\theta$, $k_y=k_r\cdot\cos\varphi, \mathrm{k}_z=k_r\cdot\sin\varphi$, and $\psi=\varphi-\theta$. Procedures of variables substitution between the two coordinates are omitted. Then, the integration becomes:

$$u^*(\omega,y,z)=\frac{1}{4\pi}\int_0^{\infty}\int_0^{2\pi}\frac{1}{k_s^2-k_r^2}e^{+ik_r\cos\psi}k_r\,d\psi dk_r \tag{2.33}$$

Bessel function of the first kind can be obtained from the above internal integration, which can be substituted by Hankel's function. In the end, the 2D Green's function can be obtained by a contour integration, i.e.,

$$u^*_{full}(\omega,\underline{x},\underline{x}_0)=\frac{-i}{4G}H_0^{(2)}(k_s r) \tag{2.34}$$

which is also represented by Hankel's function, where *G* is the shear modulus, k_s is the total wave number and *r* is the distance between the sources and the receivers. It is important to know that this is the solution in a full space. Therefore, it has to be modified by introducing a reflection point of the source point (with regard to the half-space division boundary, e.g., y-axis in this case). In this way, the influence caused by the full space can be compensated[4].The Green's function for a half-space is written as:

$$u^*_{half}(\omega,\underline{x},\underline{x}_0)=\frac{-i}{4G}[H_0^{(2)}(k_s R_1)+H_0^{(2)}(k_s R_2)] \tag{2.35}$$

with

$$R_1 = |r - r_1| = \sqrt{(y - y_0)^2 + (z - z_0)^2}$$
$$R_2 = |r - r_2| = \sqrt{(y - y_0)^2 + (z - (-z_0))^2} \tag{2.36}$$

where $R_1 = |r - r_1|$, $R_2 = |r - r_2|$ are the distances between the receiver and source point, the regarding reflected source point, respectively. Furthermore, a first derivative with respect of *r* gives the green function shear stress term. In sum, considering a unit amplitude line source, they are written as below:

$$u_x^*(\omega, \underline{x}, \underline{x}_0) = \frac{-i}{4G}[H_0^{(2)}(k_s R_1) + H_0^{(2)}(k_s R_2)] \tag{2.37}$$

One should treat the sign precisely. The Hankel's function of the second kind corresponds with the outgoing wave, and considering the inverse Fourier transform factor $\exp(i\omega t)$ .Therefore, the shear stress can be calculated by taking the first derivative of displacement,

$$\sigma_{r_1 x}^*(\omega, \underline{x}, \underline{x}_0) = G\frac{\partial u_x^*}{\partial r_1} \tag{2.38}$$

$$\sigma_{\theta_1 x}^*(\omega, \underline{x}, \underline{x}_0) = G\frac{\partial u_x^*}{\partial \theta_1} \tag{2.39}$$

Be careful that the arguments in the Hankel's function is with respect to variable R_1 and R_2, which are defined in the global coordinate. However, the derivative is with respect to local coordinate. Therefore, similar tricks are applied in order to represent shear stress along the cavity surface. Note that here two local coordinates are introduced to describe receivers and sources separately.

The Green's function displacement in Eq(2.37) are firstly converted from global coordinate into local coordinate, and then from Cartesian coordinate to polar coordinate. In the following derivation, (y_1, z_1) and (y_2, z_2) represents one receiver and one source in the global coordinate, respectively. $(y_{1,1}, z_{1,1})$ represents one receiver in the first local coordinate*(1)* and $(y_{2,2}, z_{2,2})$ represents one source in the second local coordinate*(2)*. r_1 and θ_1 represent the polar radius and angle in the first local coordinate*(1)*, which illustrates the state of the receiver points. While r_2 *and* θ_2 represent the polar radius and angle in the second local coordinate*(2)*, which describes the state of the source points. Their relation is depicted in the following graph:

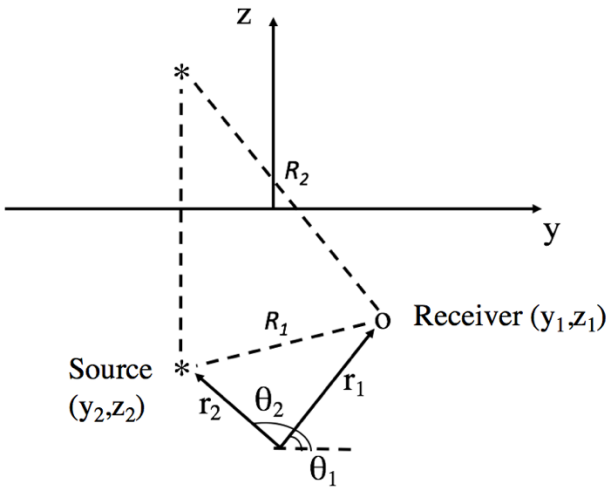

Figure 2.3 Coordinates relationship

Relationship between R_1 and r_1, R_2 and r_1 are separately derived below:

$$R_1^2 = (y_1 - y_2)^2 + (z_1 - z_2)^2 \tag{2.40}$$

And we have the conversion formula from global coordinate to local coordinate:

$$\begin{cases} y_1 = y_{1,1} \\ z_1 = z_{1,1} - H \end{cases} \qquad \begin{cases} y_2 = y_{2,2} \\ z_2 = z_{2,2} - H \end{cases} \tag{2.41}$$

In the local coordinate, coordinates can be written in the polar coordinates:

$$\begin{cases} y_{1,1} = r_1 \cos\theta_1 \\ z_{1,1} = r_1 \sin\theta_1 \end{cases} \qquad \begin{cases} y_{2,2} = r_2 \cos\theta_2 \\ z_{2,2} = r_2 \sin\theta_2 \end{cases} \tag{2.42}$$

Combining all rules stated above, R_1 can now be represented as:

$$\begin{aligned} R_1^2 &= (y_{1,1} - y_{2,2})^2 + ((z_{1,1} - H) - (z_{2,2} - H))^2 \\ &= (y_{1,1} - y_{2,2})^2 + (z_{1,1} - z_{2,2})^2 \\ &= (r_1 \cos\theta_1 - r_2 \cos\theta_2)^2 + (r_1 \sin\theta_1 - r_2 \sin\theta_2)^2 \end{aligned} \tag{2.43}$$

$$R_1 = [(r_1 \cos\theta_1 - r_2 \cos\theta_2)^2 + (r_1 \sin\theta_1 - r_2 \sin\theta_2)^2]^{\frac{1}{2}} \tag{2.44}$$

Therefore, the derivative of R_1 with respect to r_1, where the receiver is located, has the following form:

$$\frac{\partial R_1}{\partial r_1} = \frac{1}{R_1}(r_1 \cos\theta_1 - r_2 \cos\theta_2)\cos\theta_1 + \frac{1}{R_1}(r_1 \sin\theta_1 - r_2 \sin\theta_2)\sin\theta_1 \tag{2.45}$$

Using the same logic, derivative of R_1 with respect to θ_1 is also calculated, the exact form is as below:

$$\frac{\partial R_1}{\partial \theta_1} = \frac{1}{R_1}(r_1\cos\theta_1 - r_2\cos\theta_2)(-r_1\sin\theta_1) + \frac{1}{R_1}(r_1\sin\theta_1 - r_2\sin\theta_2)(r_1\cos\theta_1)$$

(2.46)

where r_1 and θ_1 depend on the positon of receiver points, while r_2 *and* θ_2 depend on the position of sources. When doing the actual calculation, r_1 and r_2 are just constant radius, depending on the location of the receivers and sources. R_1 *and* R_2 are different as the group of receivers and sources change. For R_2 in the Hankel's function argument, the same idea is applied:

$$R_2^2 = (y_1 - y_2)^2 + (z_1 + z_2)^2 \tag{2.47}$$

Substituting the relationship (2.41) and (2.42), R_2 can be rewritten as:

$$\begin{aligned} R_2^2 &= (y_{1,1} - y_{2,2})^2 + ((z_{1,1} - H) + (z_{2,2} - H))^2 \\ &= (y_{1,1} - y_{2,2})^2 + (z_{1,1} + z_{2,2} - 2H)^2 \\ &= (r_1\cos\theta_1 - r_2\cos\theta_2)^2 + (r_1\sin\theta_1 + r_2\sin\theta_2 - 2H)^2 \end{aligned}$$

(2.48)

Or in the form:

$$R_2 = [(r_1\cos\theta_1 - c_0 r_1\cos\theta_2)^2 + (r_1\sin\theta_1 + c_0 r_1\sin\theta_2 - 2H)^2]^{\frac{1}{2}} \tag{2.49}$$

Therefore, taking the derivative with respect to r_1 in the receiver coordinate gives:

$$\frac{\partial R_2}{\partial r_1} = \frac{1}{R_2}(r_1\cos\theta_1 - r_2\cos\theta_2)\cos\theta_1 + \frac{1}{R_2}(r_1\sin\theta_1 + r_2\sin\theta_2 - 2H)\sin\theta_1$$

(2.50)

Likewise,

$$\frac{\partial R_2}{\partial \theta_1} = \frac{1}{R_2}(r_1\cos\theta_1 - r_2\cos\theta_2)(-r_1\sin\theta_1) + \frac{1}{R_2}(r_1\sin\theta_1 + r_2\sin\theta_2 - 2H)(r_2\cos\theta_1)$$

(2.51)

In the end, the green function state shear stress term can be finalized with all term presented:

$$\sigma^*_{r_1 x} = \frac{i}{4}k_s[H_1^{(2)}(k_s R_1)\cdot\frac{\partial R_1}{\partial r_1} + H_1^{(2)}(k_s R_2)\cdot\frac{\partial R_2}{\partial r_1}] \tag{2.52}$$

$$\sigma^*_{\theta_1 x} = \frac{i}{4}k_s[H_1^{(2)}(k_s R_1)\cdot\frac{\partial R_1}{\partial \theta_1} + H_1^{(2)}(k_s R_2)\cdot\frac{\partial R_2}{\partial \theta_1}] \tag{2.53}$$

So far, all terms that are needed for solving the boundary integral method are presented. It is important to keep in mind the conversion of the coordinate since the displacement

imposed for derivative was defined in the global coordinate while its relating stresses are derived in the local coordinate.

2.5 Issues about Direct Boundary Integral Method

It is worth noticing that the displacement at the half space surface can not be calculated directly, therefore, a post-processing is needed. Moreover, there exists a problem in calculating the shear stresses accurately using analytical expressions.

Firstly, if we would like to calculate the displacement at the half space surface, sources are to be placed at the half space surface. Referring to the boundary integral form Eq(2.4), the body force for Green's function state is no longer zero and should be taken into account. Assuming the body force to be unit amplitude, it is written in the form

$$f_A = 1 \cdot \delta(\underline{x} - \underline{x}_0) \tag{2.54}$$

Then instead of Eq(2.7), considering state A is Green's state and state B is actual state, Eq(2.4) can be simplified as:

$$\int_S [\sigma^{sc}_{r_1 x}(\underline{x}) u^*_x(\underline{x}, \underline{x}_0) - \sigma^*_{r_1 x}(\underline{x}, \underline{x}_0) u^{sc}_x(\underline{x})] dS = \int_V 1 \cdot \delta(\underline{x} - \underline{x}_0)\, u^{sc}_x(\underline{x}) dV \tag{2.55}$$

Since Dirac-delta function is insider the integral, the right hand side of Eq(2.55) can be then integrated to:

$$\int_S [\sigma^{sc}_{r_1 x}(\underline{x}) u^*_x(\underline{x}, \underline{x}_0) - \sigma^*_{r_1 x}(\underline{x}, \underline{x}_0) u^{sc}_x(\underline{x})] dS = C_z \cdot u^{sc}_x(\underline{x}_0) \tag{2.56}$$

where C_z=1 when the sources are defined in the region V here. Otherwise, if the sources are defined outside the region V (e.g., within the cavity), then C_z=0, just like the case discussed before. Therefore, we can firstly calculate the scattered displacement at the cavity surface, and then using this result, the scattered displacement at the half space surface can be calculated.

Secondly, we may use solved scattered displacement at the cavity surface to obtain the shear stresses $\sigma_{r_1 x}$ and $\sigma_{\theta_1 x}$ based on Eq(2.7) . Then sources are to be placed around the cavity, which are located at the same positions of the receivers. This brings a singularity problem because the arguments in the Green's function stress terms will be limited to zero value. And we know that Bessel's function with a zero argument will become infinitely large. Researchers have used other techniques to overcome this issue but in this report, another form of boundary integral method is introduced below.

2.6 Indirect Boundary Integral Method

The method described in the previous sections is a direct boundary integral method, which can obtain the final displacement at the cavity surface by solving just one set of equations. However, to eliminate the limitations for calculating the shear stresses, an indirect boundary integral method is now introduced. This method is reproduced using Luco and De Barros's idea[5].

The scattered field is represented as response resulting from the action of a distribution of concentrated line loads, which locate within the region to be occupied by the cavity as shown in Figure 2.1(segmented red line). These virtual line loads are firstly solved by satisfying the traction-free boundary condition at the cavity surface Eq(2.12). Instead of responses being unknown in the previous method, now the sources are unknown and have to be firstly calculated.

$$\int_{L_1} [\sigma^*_{r_1 x}(\underline{x},\underline{x}_0) F(\underline{x}_0)] dL_1(\underline{x}_0) = -\sigma^{free}_{r_1 x}(\underline{x}) \tag{2.57}$$

where $\underline{x}_0$ is the coordinate of these line loads and $\underline{x}$ is the coordinate of the receivers located around the cavity. After solving these line loads, by means of transfer function, the displacement and shear stresses can be calculated. The scattered displacement is then written in the form

$$u^{sc}_x(\underline{x}) = \sum_{j=1}^{N_S} [u^*_x(\underline{x},\underline{x}_0) F(\underline{x}_0)] \tag{2.58}$$

And the scattered shear stresses are then written in the form

$$\sigma^{sc}_{r_1 x}(\underline{x}) = \sum_{j=1}^{N_S} [\sigma^*_{r_1 x}(\underline{x},\underline{x}_0) F(\underline{x}_0)] \tag{2.59}$$

$$\sigma^{sc}_{\theta_1 x}(\underline{x}) = \sum_{j=1}^{N_S} [\sigma^*_{\theta_1 x}(\underline{x},\underline{x}_0) F(\underline{x}_0)] \tag{2.60}$$

3. PROGRAMMING IN MATLAB

3.1 Direct Boundary Integral Method

From the previous chapters, all the terms included in the boundary integral are presented. The following steps are to solve the discretized form of boundary integral Eq(2.9),we know that the number of the equations is the number of known sources, and the number of unknowns is the number of receivers. We use *N* to represent the number of receivers and *M* number of sources. In principal, the number of receivers and number of sources do not necessarily have to be equal. For different sources, Eq(2.9) holds, therefore, if we write down all equations that are needed,

For example, for source point $i = 1$,

$$\begin{aligned}
&-\sigma^{free}_{r_1 x}(\underline{x}_1)u^*_x(\underline{x}_1,\underline{x}_{0,1}) - \sigma^*_{r_1 x}(\underline{x}_1,\underline{x}_{0,1})u^{sc}_x(\underline{x}_1)\\
&-\sigma^{free}_{r_1 x}(\underline{x}_2)u^*_x(\underline{x}_2,\underline{x}_{0,1}) - \sigma^*_{r_1 x}(\underline{x}_2,\underline{x}_{0,1})u^{sc}_x(\underline{x}_2)\ ...\\
&-\sigma^{free}_{r_1 x}(\underline{x}_N)u^*_x(\underline{x}_N,\underline{x}_{0,1}) - \sigma^*_{r_1 x}(\underline{x}_N,\underline{x}_{0,1})u^{sc}_x(\underline{x}_N) = 0
\end{aligned} \tag{3.1}$$

And for source point $i = 2$,

$$\begin{aligned}
&-\sigma^{free}_{r_1 x}(\underline{x}_1)u^*_x(\underline{x}_1,\underline{x}_{0,2}) - \sigma^*_{r_1 x}(\underline{x}_1,\underline{x}_{0,2})u^{sc}_x(\underline{x}_1)\\
&-\sigma^{free}_{r_1 x}(\underline{x}_2)u^*_x(\underline{x}_2,\underline{x}_{0,2}) - \sigma^*_{r_1 x}(\underline{x}_2,\underline{x}_{0,2})u^{sc}_x(\underline{x}_2)\ ...\\
&-\sigma^{free}_{r_1 x}(\underline{x}_N)u^*_x(\underline{x}_N,\underline{x}_{0,2}) - \sigma^*_{r_1 x}(\underline{x}_N,\underline{x}_{0,2})u^{sc}_x(\underline{x}_N) = 0
\end{aligned} \tag{3.2}$$

…

Likewise, for source point $i = M$,

$$\begin{aligned}
&-\sigma^{free}_{r_1 x}(\underline{x}_1)u^*_x(\underline{x}_1,\underline{x}_{0,M}) - \sigma^*_{r_1 x}(\underline{x}_1,\underline{x}_{0,M})u^{sc}_x(\underline{x}_1)\\
&-\sigma^{free}_{r_1 x}(\underline{x}_2)u^*_x(\underline{x}_2,\underline{x}_{0,M}) - \sigma^*_{r_1 x}(\underline{x}_2,\underline{x}_{0,M})u^{sc}_x(\underline{x}_2)\ ...\\
&-\sigma^{free}_{r_1 x}(\underline{x}_N)u^*_x(\underline{x}_N,\underline{x}_{0,M}) - \sigma^*_{r_1 x}(\underline{x}_N,\underline{x}_{0,M})u^{sc}_x(\underline{x}_N) = 0
\end{aligned} \tag{3.3}$$

N unknowns and *M* equations are presents. All known terms can be moved to the right hand side of the equations and the equation set can be rewritten in a matrix form. In the end, the equations are constructed in a more intuitive manner:

$$\begin{bmatrix} \sigma^*_{r_1x}(\underline{x}_1,\underline{x}_{0,1}) & \sigma^*_{r_1x}(\underline{x}_2,\underline{x}_{0,1}) & \dots & \sigma^*_{r_1x}(\underline{x}_N,\underline{x}_{0,1}) \\ \sigma^*_{r_1x}(\underline{x}_1,\underline{x}_{0,2}) & \sigma^*_{r_1x}(\underline{x}_2,\underline{x}_{0,2}) & \dots & \sigma^*_{r_1x}(\underline{x}_N,\underline{x}_{0,2}) \\ & & \dots & \\ \sigma^*_{r_1x}(\underline{x}_1,\underline{x}_{0,M}) & \sigma^*_{r_1x}(\underline{x}_2,\underline{x}_{0,M}) & \dots & \sigma^*_{r_1x}(\underline{x}_N,\underline{x}_{0,M}) \end{bmatrix} \cdot \begin{bmatrix} u^{sc}_x(\underline{x}_1) \\ u^{sc}_x(\underline{x}_2) \\ \dots \\ u^{sc}_x(\underline{x}_N) \end{bmatrix} =$$

$$\begin{bmatrix} \sigma^{free}_{r_1x}(\underline{x}_1)u^*_x(\underline{x}_1,\underline{x}_{0,1}) + \sigma^{free}_{r_1x}(\underline{x}_2)u^*_x(\underline{x}_2,\underline{x}_{0,1}) + \dots + \sigma^{free}_{r_1x}(\underline{x}_N)u^*_x(\underline{x}_N,\underline{x}_{0,1}) \\ \sigma^{free}_{r_1x}(\underline{x}_1)u^*_x(\underline{x}_1,\underline{x}_{0,2}) + \sigma^{free}_{r_1x}(\underline{x}_2)u^*_x(\underline{x}_2,\underline{x}_{0,2}) + \dots + \sigma^{free}_{r_1x}(\underline{x}_N)u^*_x(\underline{x}_N,\underline{x}_{0,2}) \\ \dots \\ \sigma^{free}_{r_1x}(\underline{x}_1)u^*_x(\underline{x}_1,\underline{x}_{0,M}) + \sigma^{free}_{r_1x}(\underline{x}_2)u^*_x(\underline{x}_2,\underline{x}_{0,M}) + \dots + \sigma^{free}_{r_1x}(\underline{x}_N)u^*_x(\underline{x}_N,\underline{x}_{0,M}) \end{bmatrix}$$

(3.4)

The matrix form has the form $\underline{\underline{A}}_{M\times N} \cdot \underline{X}_{N\times 1} = \underline{B}_{M\times 1}$ where matrix $\underline{\underline{A}}$ can be regarded as 'stiffness' matrix by analogy, where each element $A_{i,j}$ physically means the Green's function stress response at point *j* due to the excitation at point *i*. Solving these equations, we will obtain the scattered field displacement. Finally, we can obtain the total wave field as a summation of free field and the scattered field. However, using this equation set alone, we cannot obtain the response at the half-space surface because it will give a s right hand side equal to zero. Also, the shear stresses can only be calculated numerically through the displacement.

3.2 Indirect Boundary Integral Method

For indirect boundary integral method, he programming idea is reversed. In this case, the *M* sources are the unknowns to be solved. For each single receiver, Eq(2.58) holds therefore a similar 'stiffness' matrix can be constructed, which is just the transpose of the matrix $\underline{\underline{A}}$. The problem to be solved is $(\underline{\underline{A}}_{M\times N})^T \cdot \underline{X}_{M\times 1} = \underline{B}_{N\times 1}$, i.e.,

$$\begin{bmatrix} \sigma^*_{r_1x}(\underline{x}_1,\underline{x}_{0,1}) & \sigma^*_{r_1x}(\underline{x}_1,\underline{x}_{0,2}) & \dots & \sigma^*_{r_1x}(\underline{x}_1,\underline{x}_{0,M}) \\ \sigma^*_{r_1x}(\underline{x}_2,\underline{x}_{0,1}) & \sigma^*_{r_1x}(\underline{x}_2,\underline{x}_{0,2}) & \dots & \sigma^*_{r_1x}(\underline{x}_2,\underline{x}_{0,M}) \\ & & \dots & \\ \sigma^*_{r_1x}(\underline{x}_N,\underline{x}_{0,1}) & \sigma^*_{r_1x}(\underline{x}_N,\underline{x}_{0,2}) & \dots & \sigma^*_{r_1x}(\underline{x}_N,\underline{x}_{0,M}) \end{bmatrix} \cdot \begin{bmatrix} F(\underline{x}_1) \\ F(\underline{x}_2) \\ \dots \\ F(\underline{x}_M) \end{bmatrix} = \begin{bmatrix} \sigma^{free}_{r_1x}(\underline{x}_1) \\ \sigma^{free}_{r_1x}(\underline{x}_2) \\ \dots \\ \sigma^{free}_{r_1x}(\underline{x}_N) \end{bmatrix}$$

(3.5)

After these *M* unknown line loads are solved, unknown displacement at *N* receivers can be calculated by using Eq(2.59).

$$\begin{bmatrix} u_x^*(\underline{x}_1,\underline{x}_{0,1}) & u_x^*(\underline{x}_1,\underline{x}_{0,2}) & \dots & u_x^*(\underline{x}_1,\underline{x}_{0,M}) \\ u_x^*(\underline{x}_2,\underline{x}_{0,1}) & u_x^*(\underline{x}_2,\underline{x}_{0,2}) & \dots & u_x^*(\underline{x}_2,\underline{x}_{0,M}) \\ & & \dots & \\ u_x^*(\underline{x}_N,\underline{x}_{0,1}) & u_x^*(\underline{x}_N,\underline{x}_{0,2}) & \dots & u_x^*(\underline{x}_N,\underline{x}_{0,M}) \end{bmatrix} \cdot \begin{bmatrix} F(\underline{x}_1) \\ F(\underline{x}_2) \\ \dots \\ F(\underline{x}_M) \end{bmatrix} = \begin{bmatrix} u_x^{sc}(\underline{x}_1) \\ u_x^{sc}(\underline{x}_2) \\ \dots \\ u_x^{sc}(\underline{x}_N) \end{bmatrix}$$

(3.6)

Unknown shear stresses at N receivers can be calculated by using Eq(2.60) and Eq(2.61),

$$\begin{bmatrix} \sigma_{r_1x}^*(\underline{x}_1,\underline{x}_{0,1}) & \sigma_{r_1x}^*(\underline{x}_1,\underline{x}_{0,2}) & \dots & \sigma_{r_1x}^*(\underline{x}_1,\underline{x}_{0,M}) \\ \sigma_{r_1x}^*(\underline{x}_2,\underline{x}_{0,1}) & \sigma_{r_1x}^*(\underline{x}_2,\underline{x}_{0,2}) & \dots & \sigma_{r_1x}^*(\underline{x}_2,\underline{x}_{0,M}) \\ & & \dots & \\ \sigma_{r_1x}^*(\underline{x}_N,\underline{x}_{0,1}) & \sigma_{r_1x}^*(\underline{x}_N,\underline{x}_{0,2}) & \dots & \sigma_{r_1x}^*(\underline{x}_N,\underline{x}_{0,M}) \end{bmatrix} \cdot \begin{bmatrix} F(\underline{x}_1) \\ F(\underline{x}_2) \\ \dots \\ F(\underline{x}_M) \end{bmatrix} = \begin{bmatrix} \sigma_{r_1x}^{sc}(\underline{x}_1) \\ \sigma_{r_1x}^{sc}(\underline{x}_2) \\ \dots \\ \sigma_{r_1x}^{sc}(\underline{x}_N) \end{bmatrix}$$

(3.7)

$$\begin{bmatrix} \sigma_{\theta_1x}^*(\underline{x}_1,\underline{x}_{0,1}) & \sigma_{\theta_1x}^*(\underline{x}_1,\underline{x}_{0,2}) & \dots & \sigma_{\theta_1x}^*(\underline{x}_1,\underline{x}_{0,M}) \\ \sigma_{\theta_1x}^*(\underline{x}_2,\underline{x}_{0,1}) & \sigma_{\theta_1x}^*(\underline{x}_2,\underline{x}_{0,2}) & \dots & \sigma_{\theta_1x}^*(\underline{x}_2,\underline{x}_{0,M}) \\ & & \dots & \\ \sigma_{\theta_1x}^*(\underline{x}_N,\underline{x}_{0,1}) & \sigma_{\theta_1x}^*(\underline{x}_N,\underline{x}_{0,2}) & \dots & \sigma_{\theta_1x}^*(\underline{x}_N,\underline{x}_{0,M}) \end{bmatrix} \cdot \begin{bmatrix} F(\underline{x}_1) \\ F(\underline{x}_2) \\ \dots \\ F(\underline{x}_M) \end{bmatrix} = \begin{bmatrix} \sigma_{\theta_1x}^{sc}(\underline{x}_1) \\ \sigma_{\theta_1x}^{sc}(\underline{x}_2) \\ \dots \\ \sigma_{\theta_1x}^{sc}(\underline{x}_N) \end{bmatrix}$$

(3.8)

This indirect boundary integral method can be used to calculate the displacement at the half space surface. Also, the shear stress can be calculated analytically by using the transfer function. From this point, all following results that are shown are based on this method.

3.3 Parameters

In this report, a two-dimensional cavity with radius 5 meter buried under different conditions will be considered. The half space consists of linear homogeneous singled-layer soil, moreover, damping is not considered in case. The unlined cavity and half space are excited by plane SH wave from below. The space is truncated with limited width and depth so one can see the response in the vicinity surrounding the cavity. A shallow buried cavity and its corresponding discretized model are shown below:

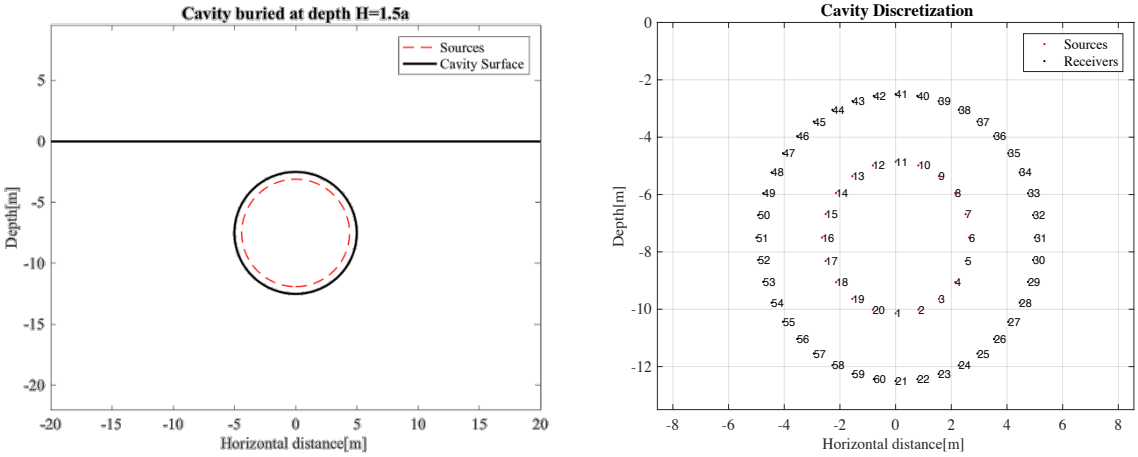

Figure 3.1 Cavity description

The origin is set to be located at *(0,0)* on the ground surface and the center of the cavity is set below y axis. The cavity surface is described by a series of black dots where locate the receivers, and the sources are placed at a radius slightly smaller than the cavity radius r_0. The angle in the local coordinate originated at *(-H,0)* will be first discretized, based on which the coordinates of receivers and sources are defined. The quantities of receivers and sources do not have to be equal, but it will influence the conditioning numbers of the 'stiffness' matrix and further phenomenon will be further discussed in the next section. A frequency dimensionless parameter η is introduced and it has the following relation with angular frequency[5]:

$$\eta = \frac{a}{c_s \pi} \omega \tag{3.9}$$

The main variables in the study are the depth of the cavity buried underground, and the frequency at which the SH wave is excited. In all case, incident angle 90 degrees is mainly investigated, where the plane SH wave is propagating exactly perpendicular to the ground surface (i.e., vertical incident wave). This can be seen as a one dimensional case. More detailed parameters are shown below:

Table 3.1 Parameters

Density ρ	1932 [kg/m^3]	
Shear modulus G	32670000 [MPa]	
Wave speed c_s	130 [m/s]	
Incident wave angle φ	90 [degrees]	
Cavity radius a	5 [m]	
Depth Radius ratio H/a	1.5	5
Dimensionless frequency η	0.5	1.0
Frequency ω	40.8[rad/s]	81.6[rad/s]

3.4 Results and Discussion

3.4.1 Convergence Tests

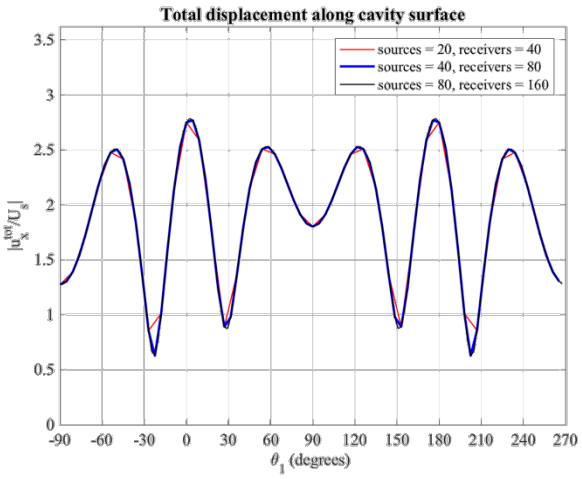

Figure 3.2 Convergence test example

Convergence tests for indirect boundary integral method were firstly carried out to make the results accurate enough to be judged. One example is shown in figure 3.2, displacement around the cavity surface in the case where depth/radius ratio is 5.0, and the excitation dimensionless frequency is 1.0. The results of displacement are normalized by the amplitude of incident motion, $\left|U_x^{cav}\right| = \left|U_x^{tot} / U_s\right|$.

As suggested in the study presented by Luco and De Barros[5], the number of sources and receivers are set to be 20/40,40/80 and 80/160, respectively. It can be seen from the graph that the first case 20/40 does not suffice to describe the results while 40/80 combination has equally good results as 80/160 combination. Therefore, in general, 40 receiver points and 80 source points are sufficient for most applications. This is also true for their study.

Furthermore, table 3.2 has shown results from more convergence tests of displacement. Besides equal number of sources and receivers, convergence tests have been carried out for unequal number of sources and receivers. The two studies show both similarities and differences.

Table 3.2 Convergence tests of displacement

	$\eta = 0.5$			$\eta = 1.0$		
Location	***H=1.5a***					
	N_S / N_O			N_S / N_O		
$\theta_1 = -90^\circ$	**20/40**	**40/80**	**80/160**	**20/40**	**40/80**	**80/160**
	1.3519	1.3519	1.3519	2.2974	2.2974	2.2974
	40/40	**80/80**	**160/160**	**40/40**	**80/80**	**160/160**
	1.3519	1.3519	1.3519	2.2974	2.2974	2.2974
$\theta_1 = 0^\circ$	**20/40**	**40/80**	**80/160**	**20/40**	**40/80**	**80/160**
	1.8668	1.9032	1.9203	0.5988	0.5352	0.5152
	40/40	**80/80**	**160/160**	**40/40**	**80/80**	**160/160**
	1.9368	1.9368	1.9368	0.5042	0.5042	0.5042
Location	***H=5a***					
	N_S / N_O			N_S / N_O		
$\theta_1 = -90^\circ$	**20/40**	**40/80**	**80/160**	**20/40**	**40/80**	**80/160**
	1.8188	1.8188	1.8188	1.2748	1.2749	1.2749
	40/40	**80/80**	**160/160**	**40/40**	**80/80**	**160/160**
	1.8188	1.8188	1.8188	1.2749	1.2749	1.2749
$\theta_1 = 0^\circ$	**20/40**	**40/80**	**80/160**	**20/40**	**40/80**	**80/160**
	0.2102	0.2230	0.2427	2.7862	2.7745	2.7637
	40/40	**80/80**	**160/160**	**40/40**	**80/80**	**160/160**
	0.2686	0.2686	0.2686	2.7499	2.7499	2.7499

For both two studies, it can be judged that convergence tests showed differences at different points, it is hard to converge at the points where peak values have occurred. Convergence is easier obtained at $\theta_1 = -90^\circ$ compared to $\theta_1 = 0^\circ$ on the cavity. Therefore, at those peak value points, more numbers are suggested depending on the accuracy demands. Secondly, for high frequency cases, more peaks and oscillation patterns will appear on the graphs, it is advisable to use more points to capture the cavity responses. It has been tested that at even higher frequency where dimensionless frequency is equal to 3.0, combination of 80/160 or 160/160 are proven to be sufficient. (Results not shown here) In the following sections, combination of 160/160 is used to obtain a smooth curve unless specified.

Combination of equal observations and sources will provide better convergence, even at the points where peak values occur. For equal number case, convergence is

satisfactory at $\theta_1 = -90^\circ$ as well as $\theta_1 = 0^\circ$. Results are easier to converge compared to unequal number cases. However, it will be shown later on that 'stiffness' matrix will have better conditioning numbers for the unequal case compared to the equal case. Another possibly reason for Luco and De Barros to use unequal numbers could be also to reduce the size of matrixes when the difference in results are not very evident. This can be further verified by looking at the calculation time for different cases: The calculation using unequal number of sources and receivers will consume less time than using equal number. This time difference is more distinctive when using large numbers.

Table 3.3 Calculation time [in seconds]

H=1.5a	$\eta = 0.5$		$\eta = 1.0$	
N_S / N_O	U_x^{Cav}	$\sigma_{\theta_1 x}$	U_x^{Cav}	$\sigma_{\theta_1 x}$
40/80	0.852	0.982	0.893	1.001
80/160	1.019	1.250	1.002	1.227
80/80	0.931	1.100	0.969	1.073
160/160	1.194	1.544	1.263	1.601

(Computer: Processor 2.7 GHz, Intel Core i5, Memory 8 GB 1867 MHz DDR3, Macbook Pro)

3.4.2 Results comparison and discussion

A comparison between numerical results calculated by the indirect boundary integral method stated above and results provided by Luco and De Barros is made. Note that they are both indirect boundary integral methods. Results for displacement on the half space surface, displacement on the cavity surface, and shear stress on the cavity surface are shown below:

1) Total displacement at half space surface.

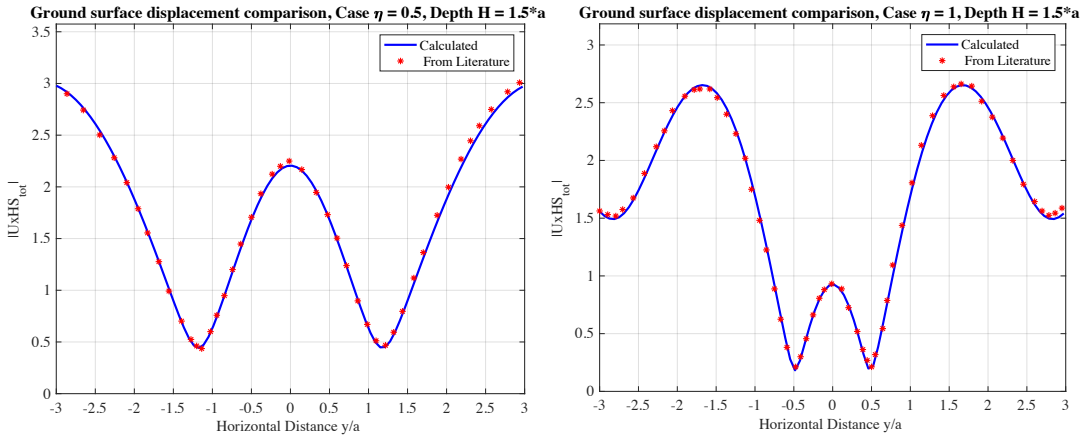

(a) (b)

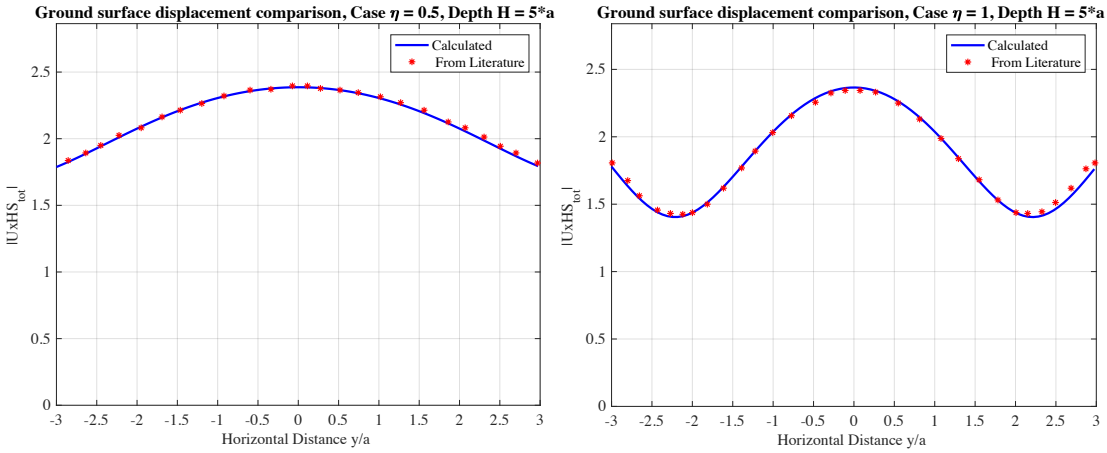

(c) (d)

Figure 3.3 Displacements comparison

In Figure 3.3, normalized displacements at the half space surface for a vertically incident SH wave (incident angle $\varphi = 90^\circ$) are shown for two different cavity depths H/a=1.5 and H/a=5.0, and for two different frequencies, $\eta = 0.5$ and $\eta = 1.0$.

Firstly, for different depth at the same frequency, for example, comparing (a) and (c), it can be seen that cavity buried at shallow depth will give more 'disturbance' on the particle motion on the half space surface. The phenomenon could be explained by looking at the wave length and the depth of the cavity. In this situation, incident wave is reflected back from the free half space surface with the same wave length in the two cases, however, due to the difference of travel distance, they lead to different displacements because they land on different positions at one propagating wave. Secondly, for the same depth but with different frequency, for example, comparing (a) and (b), particles tend to move more intensely due to the fact that high frequency excitation gives shorter wave length.

Comparing to the results obtained by Luco and De Barros, the method presented in this report shows a very good consistency. Like stated before, it is advised to use a larger number of points in order to capture a sharp displacement change between two peaks.

2) Total displacement at cavity surface.

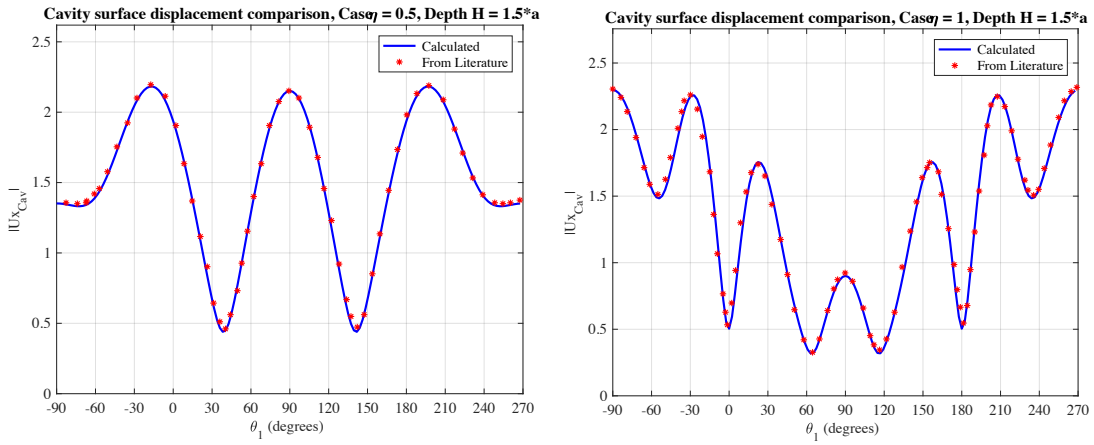

(a) (b)

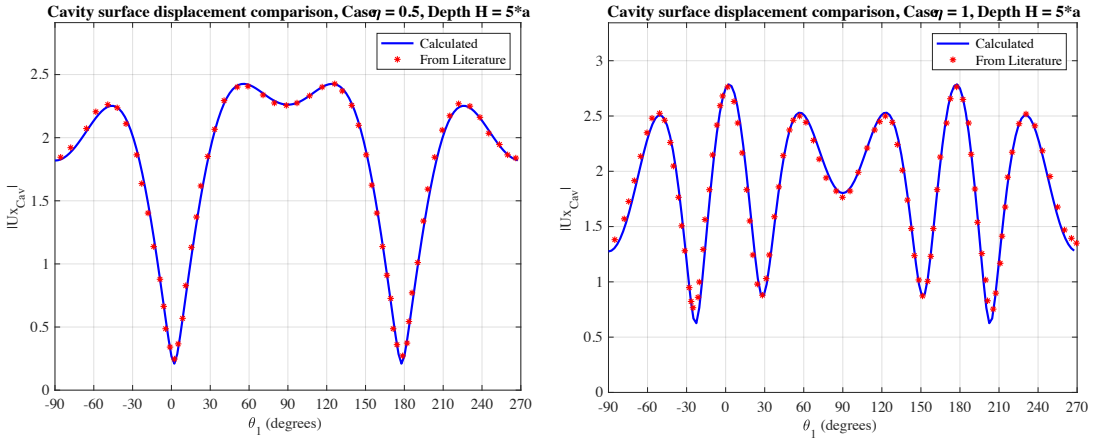

(c) (d)

Figure 3.4 Displacements comparison

In Figure 3.4, similar to the results shown above, displacements around the cavity surface for a vertically incident SH wave (incident angle $\varphi = 90^\circ$) are also shown for two different cavity depths and for two different frequencies. The results of displacement are also normalized by the amplitude of incident motion. Displacements around the cavity are shown with θ_1 varying from -90 degree to 270 degree.

Referring to Figure 1.1, It can be verified that displacement around the cavity surface should be polar symmetric with regard to $\theta_1 = 90^\circ$ since the imposed incident wave coming from below is perpendicular to the half space surface. For other cases where incident angle $\varphi \neq 90^\circ$, it should be clear that the displacement does not necessarily have to be polar symmetric with regards to $\theta_1 = 90^\circ$. Judging from the graphs above, the maximum displacement could occur at anywhere around the cavity. The response relates to the parameters, including the depth of the cavity, excitation frequency (Both are investigated in this report), geometry of the cavity, incident wave angle and soil parameters. Here, the response of the displacement around the cavity is more sensitive to excitation frequency than to the influence of changing the depth of the cavity.

Similarly, results from the literature and results calculated by using the reciprocity based boundary integral method show a good consistency.

3) Total shear stress $S_{\theta_1 x}$ comparison.

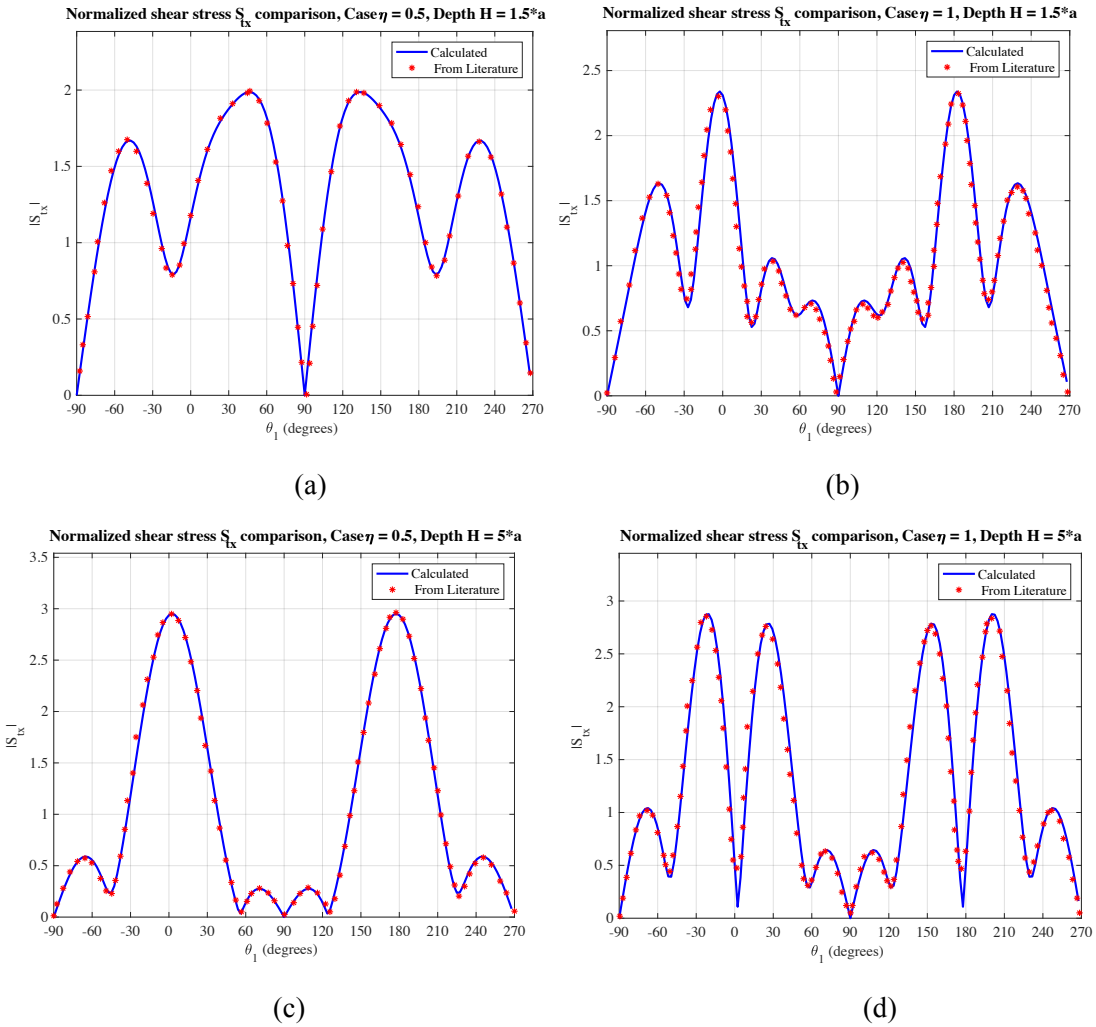

Figure 3.5 Shear stresses comparison

The amplitude of the normalized total shear stress $|S_{tx}| = |S_{\theta_1 x} / \omega \rho c_s U_s|$ along the cavity wall is shown above. The total shear stresses are calculated by use of Eq(2.26) and Eq(2.53) from the field field and scattered field, respectively.

Comparing cases for low and high frequency, (a) and (b) for example, more peaks will appear for the high frequency case which means the particle motion along the cavity wall will be more vigorous and unstable.

Comparing to the literature data provided, the results calculated have a slight difference. For example, one can observe a tiny shift for (b) and for (d), the anti-peaks at 0° and 180° do not coincide. However, it has been checked that results calculated here have a good reliability.

3.4.3 Boundary conditions check

Boundary conditions must be checked to verify the credibility of the results. As stated before, there are two boundary conditions in this problem, i.e., traction-free at the half space surface (which has been already satisfied by assuming the same amplitude for incoming waves and reflected waves from the surface), traction-free at the cavity wall surface (which will be checked in this section). The total shear stresses are calculated by use of Eq(2.25) and Eq(2.52) from the free field and scattered field respectively. Theoretically, their sum should be exactly zero in order to satisfy the boundary condition, however, due to numerical calculation accuracy, the closer it is to zero, the better the boundary condition is satisfied. A post-processing gives the following graphs:

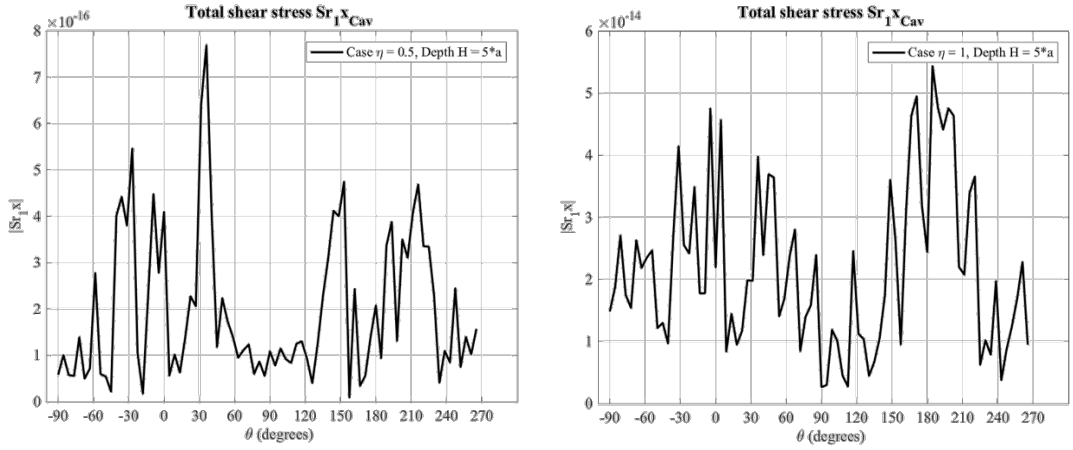

Figure 3.6 Boundary conditions check

Boundary conditions are checked for large depth case in terms of low frequency and high frequency. The total shear stress $S_{r_1 x}$ is also normalized therefore it can be seen clearly that the maximum magnitude of total stress is marginally small and neglected. Conclusion can be drawn that boundary conditions are very well satisfied by using this method.

In order to study the frequency influence on the boundary condition, the total shear stress at the cavity lowest point $\theta_1 = -90^\circ$ is plotted with varying excitation frequency as shown in Figure 3.7

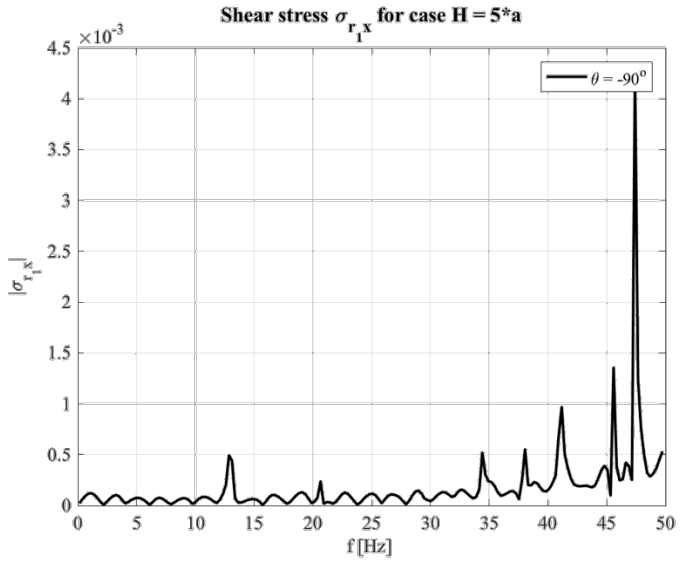

Figure 3.7 Boundary conditions with varying frequency

It can be seen that as the frequency increases, the normalized shear stress is increasing as well, thus, the boundary condition is not satisfied as well as in lower frequency case. This maximum magnitude shoots up from 10^{-16} to 10^{-3}. Moreover, it has been checked that if the number of observation and receiver points are increased, the conditioning number will increase and the boundary condition check will be even worse. (Results not shown here).

3.4.3 Frequency response function(FRF)

a) Frequency response function(FRF) at half space surface

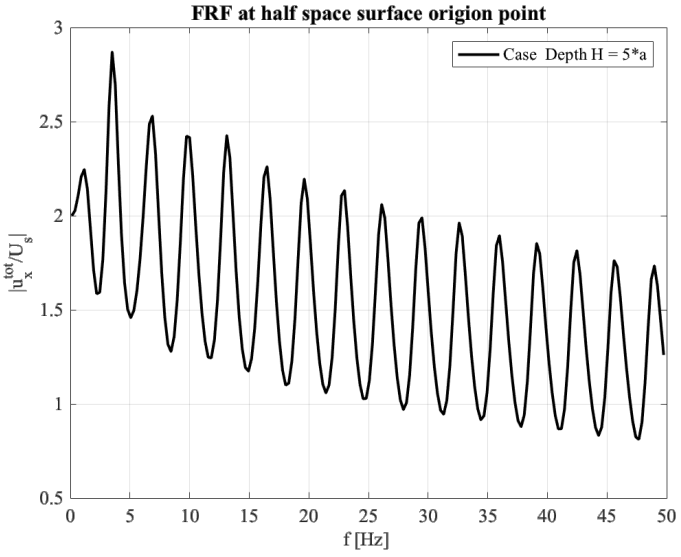

Figure 3.8 FRF at half space surface

In the graph, those peaks occurring at different frequencies represent resonances of the soil. The frequency response function can be used to find the maximum soil response at its regarding frequency, which is around 4 Hz. As can be seen from the graph, the starting point at frequency nearly equal to zero indicates a value of 2 here. It was discussed that the amplitude of the particle motion excited by free field is also 2 (incident wave plus reflected wave). Therefore, when the excitation frequency is really low, the effect of the scattered wave field is also little. When the frequency is increased, scattered wave field brought by the cavity has more influence on the total field. It is also observed that the mean value of the displacement is descending as the frequency is increasing.

b) Frequency response function(FRF) at cavity surface

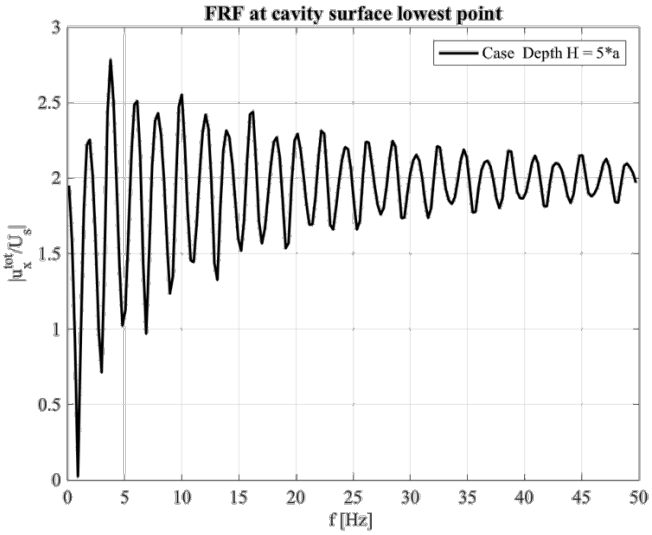

Figure 3.9 FRF at cavity surface

Frequency response function for the lowest point $\theta_1 = -90^\circ$ at the cavity is also shown in Figure 3.9. It is interesting to note the soil response at specific frequencies: At frequency equal to around 1 Hz, the normalized amplitude is nearly zero which means the particle barely vibrate. At frequency around 4Hz, the maximum normalized displacement occurs. As the frequency increases, the displacement is approaching a constant value which is approximately 2 and the deviation from the mean value also decreases.

3.4.4 Displacement in the vicinity of the cavity

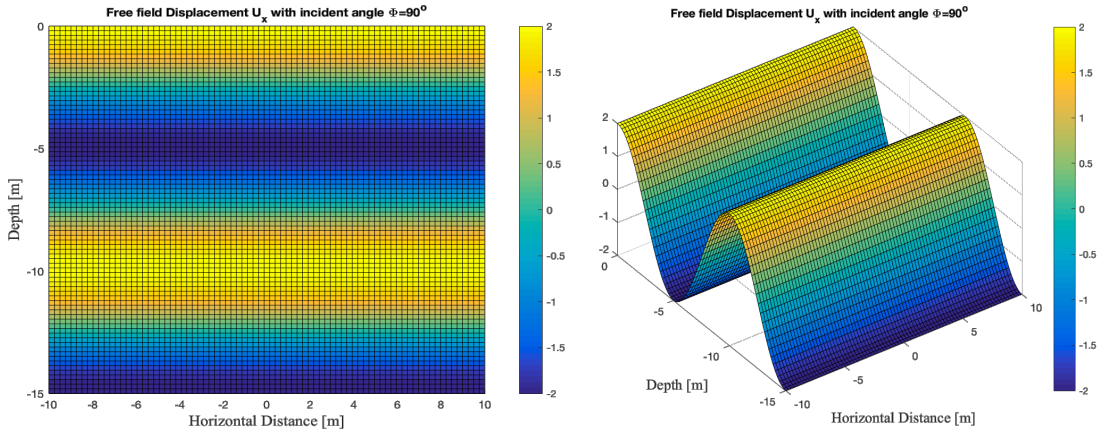

(a) *(b)*

Figure 3.10 Free wave field ($\eta = 1.0$)(a)2D plot; (b)3D plot

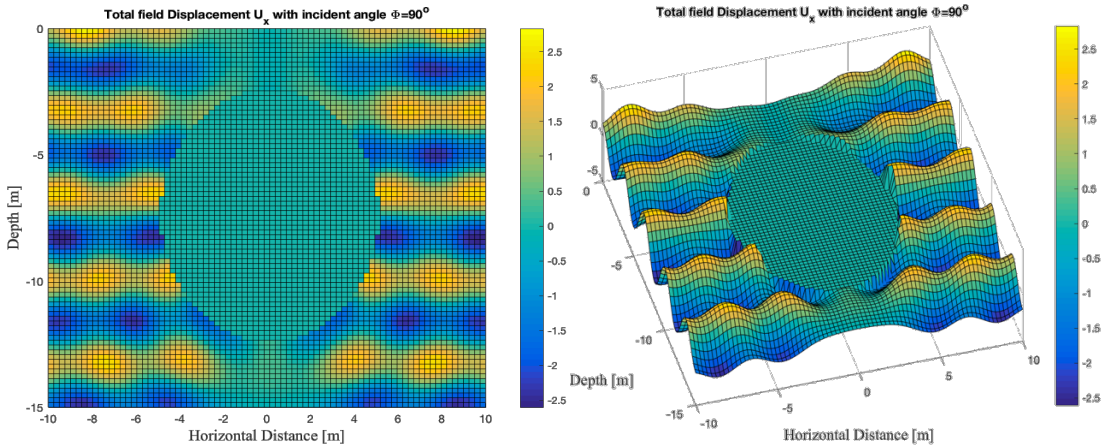

(a) *(b)*

Figure 3.11 Total wave field ($\eta = 3.0$) (a)2D plot; (b)3D plot

For comparison, the real parts of displacement in free wave field and in total wave field are both shown in Figure 3.10 and Figure 3.11, respectively. It is a cavity buried at depth H=5a. Same as the previous cases, the incident angle is chosen to be perpendicular to the half space surface.

In Figure 3.10, The free wave field is a summation of incident wave and reflected wave, and due to the interference of incident wave and reflected wave at the half space surface, the magnitude of the incident wave doubled. Therefore, constant value equal to 2 can be observed on the half space surface which is expected for plane waves. In other case where incident angle is not 90 degrees, there will be interference of incident wave field and reflected wave field. For example, some parts will be added and other parts

deducted, depending on the incident wave angle.

Figure 3.11 shows many differences: Firstly, a higher excitation frequency indicates shorter wave length. This can be well observed by looking at the distances between two peaks (yellow lines) in Figure 3.10 and in Figure 3.11. It should be noted that since the incident angle is perpendicular to the half space surface, the problem itself should be strictly symmetric, which can be used to checked the results. Secondly, particle displacements within the cavity does not exist thus is set to be zero. Due to the presence of the cavity, particles motion is not exactly the same on the same depth, compared to the propagating plane wave in the free wave field case. Thirdly, apparently the scattered wave field brought by the cavity will greatly influence the particle displacement right above the cavity and right below the cavity, which may also depend on the incident wave angle.

3.4.5 Conditioning numbers

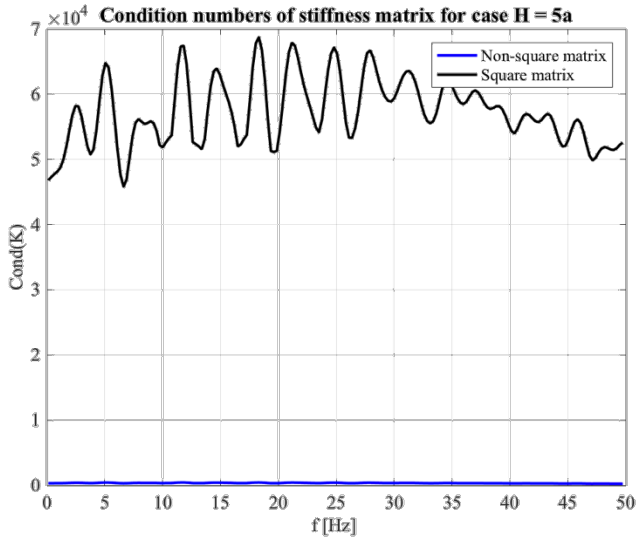

Figure 3.12 Conditioning numbers comparison

One may be curious to study the influence of 'stiffness' matrix, which was presented in Eq(3.4), being square or non-square. Therefore, the conditioning numbers are plotted for the two cases, 80/160 for the blue line and 160/160 for the black line, with varying frequencies. Firstly, it is shown that the varying frequency does not change too much the conditioning numbers which stay at a rather 'constant' level. Secondly, a non-square matrix could give much smaller conditioning numbers compared to a square matrix in all frequencies, which is around 400. Therefore, a non-square matrix is well-conditioned while a square matrix is ill-conditioned. This means small errors in the input will cause small change in the output so the results calculated by a non-square

matrix is less sensitive to perturbation, therefore more reliable. This further explains why Luco and De Barros would rather use a non-square matrix.

4. CONCLUSION

The reciprocity theorem has been briefly introduced, based on which a direct boundary integral method has been introduced. Scattered wave field for a cavity embedded in the 2D half space can be solved by means of using this method. The procedure for calculating the free field and 2D Green's function has been explicitly illustrated.

Although the displacement at the cavity surface can be solved at once, the limitations of the direct boundary integral method are eliminated by applying indirect boundary integral method, which is reproduced by referring to a classical study from Luco and De Barros. Programming process in MATLAB has been explicitly shown, and in the end, results using indirect boundary integral method are calculated.

Convergence tests show that a square 'stiffness' matrix gives a better converged result, however, a non-square matrix can give smaller conditioning numbers. Comparison between the calculated results obtained by using this indirect method and results provided by the literature has shown that the obtained results have really good consistency and are reasonably accurate. Boundary conditions have been checked to be fairly good. Furthermore, more post processed results, e.g., transfer functions, are shown and they might be useful for engineering practice.

5. LITERATURE

[1] Paul Holscher, (2016). Soil dynamics in urban areas. Delft University of Technology.

[2] Achenbach, J. D. (2003). Reciprocity in elastodynamics. Cambridge University Press.

[3] Graff, K. F. (2012). Wave motion in elastic solids. Courier Corporation.

[4] Kausel, E. (2006). Fundamental solutions in elastodynamics: a compendium. Cambridge University Press.

[5] Luco, J. E., & De Barros, F. C. P. (1994). Dynamic displacements and stresses in the vicinity of a cylindrical cavity embedded in a half-space. Earthquake engineering & structural dynamics, 23(3), 321-340.

6. APPENDIX

An original version of direct boundary integral method programming codes is pasted below, it can be only used to calculate the total displacement along the cavity surface and does not account for calculating displacements on the half space surface and shear stresses. Also, the post processing for results shown in the report is not included in this original script.

Code:

```
% (c)Jun Yuan
% The boundary integral method is used to obtain the two-dimensional response
% of a cylindrical cavity embedded in a uniform elastic half space subjected to SH wave.
%=========================================================================
==

clear all;
close all;

%% Discretize the cacity & Define the location of sources ( store in [x_0,y_0]) and observations ( store
in [x,y])
a   =   5;                  % Consider the cavity as a circle, define the radius of the cavity a
H   =   1.5*a;              % The ratio of the depth of the cavity to the radius of the cavity
n_ps    =   40;             % Number of source points
n_po    =   40;             % Number of observation points along the cavity surface
Ng      =   40;             % Number of observation points along the ground surface [-3<y<3,0]
Eta     =   0.5;            % Dimensioness frequency
Phi     =   pi/2;           % Angle between wave propagation direction and y-axis

% Define the position of receivers along the cavity surface
Sego    =   n_po;           % Number of segments of observation points
rcz     =   -H;
rcy     =   0;              % Position of the circle center [rcy,rcz] is (-H,0)
dtta1   =   2*pi/Sego;                  % Increment of the angle for receivers points
tta1    =   (-0.5*pi):dtta1:(1.5*pi-dtta1);
y       =       a*cos(tta1);
z       =   rcz + a*sin(tta1);          % [y,z] is the coordinate of receivers points

% Define the position of sources slightly inside the cavity surface
Segs        =   n_ps;                   % Number of segments
ap          =   a* (1 -( 3*2*pi)/ n_po);    % Define the radius of the source, which is
```

```
slightly smaller than that of the recievers
dtta2          =   2*pi/Segs;                          % Increment of the angle at sorces points
tta2           =   (-0.5*pi):dtta2:(1.5*pi-dtta2);
y0             =            ap*cos(tta2);
z0             =   rcz + ap*sin(tta2);                % [y0,z0] is the coordinate of sources points

%% Material Properties
rho            =   1932;                               % Density of the soil
G              =   3.26e7;                             % Shear modulus
cs             =   sqrt(G/rho);                        % Wave speed
omega          =   Eta*pi*cs/a;                        % Excitation frequency
ks             =   omega/cs;                           % Total wave number
ky             =   ks * cos(Phi);                      % Wave number in y direction
kz             =   ks * sin(Phi);                      % Wave number in z direction

%% Define shear stress term in free wave field
U_0            =   1 ;                                 % the amplitude of plane wave in free wave field
ux_free        =   zeros(n_po,1);                      % Array to store displacement in free wave field
sigma_r1x_free =   zeros(n_po,1);                      % Array to store shear stress in free wave field

for j = 1:n_po
    ux_free(j)        =   U_0 * (exp(-1i*kz*z(j)-1i*ky*y(j)) + exp(+1i*kz*z(j)-1i*ky*y(j)));
    sigma_r1x_free(j) =   G*U_0* ((-1i*ky)*cos(tta1(j))+ (-1i*kz)*sin(tta1(j))) * exp(-1i*kz*z(j)-
1i*ky*y(j))...
                        + G*U_0* ((-1i*ky)*cos(tta1(j))+ (+1i*kz)*sin(tta1(j))) *
exp(+1i*kz*z(j)-1i*ky*y(j));
end
sigma_r1x_sca  = -sigma_r1x_free;                      % Array to store shear stress in scattered wave field

%% Define 2D Green's function
R1             = zeros(n_ps,n_po);                     % Matrix to store the distances between the sources
and receivers
R2             = zeros(n_ps,n_po);                     % Matrix to store the distances between the reflected
sources and receivers
ux_star        = zeros(n_ps,n_po);                     % Matrix to store the green function displacements
sigmar1x_star = zeros(n_ps,n_po);                      % Matrix to store the green function shear stresses
%set up the 'stiffness' matrix for green function state A, at one frequency
%sigma_rx_star[i,j] means the response at the receiver point i due to
%source at point j.
```

```
for s = 1:n_ps
    for r = 1:n_po
        R1(s,r) = sqrt((y(r)-y0(s))^2+(z(r)-z0(s))^2);
        R2(s,r) = sqrt((y(r)-y0(s))^2+(z(r)+z0(s))^2);
        ux_star(s,r) = (-1i/4/G)*(besselh(0,2,ks*R1(s,r))+ besselh(0,2,ks*R2(s,r)));

        %a is r1 at response points, theta1 is tta1,
        %ap is r2 at source points, theta2 is tta2.
        s1 = (a*cos(tta1(r)) - ap*cos(tta2(s)))* cos(tta1(r)) ;
        s2 = (a*sin(tta1(r)) - ap*sin(tta2(s)))* sin(tta1(r)) ;
        s3 = (a*cos(tta1(r)) - ap*cos(tta2(s)))* cos(tta1(r)) ;
        s4 = (a*sin(tta1(r)) + ap*sin(tta2(s))- 2*H) * sin(tta1(r)) ;
        sigmar1x_star(s,r) = ks*(1i/4)*(s1+s2)/R1(s,r)*besselh(1,2,ks*R1(s,r))+
ks*(1i/4)*(s3+s4)/R2(s,r)* besselh(1,2,ks*R2(s,r));
    end
end

%% Core algorithm for calcutating the response

% For one fixed source j , formulate boundary integral.

%%Solve the linear algebraic equations in the form of matrix    Ax=B
A1 = -sigmar1x_star;                    % Matrix to store the coefficients, dimension
[Nsource*Nreceivers]
B1 = zeros(n_ps,1);                     % Matrix to store the unknown scattered displacements

for i = 1:n_ps                          % for each source(row), add all the terms to become a B(i)
    acc = 0;
    for j = 1:n_po
        acc = sigma_r1x_free(j,1)* ux_star(i,j);
        B1(i,1) = acc + B1(i,1);
    end
end
ux_sca=A1\B1;


%In the end, the response along the cavity surface can be plotted.
ux_tot = ux_sca + ux_free;
% Matrix to store the total displacements
```

```
%% Plotting results
%%normalized by incident response at the ground surface at (0,0), i.e, ux/Us (Us=1)
figure;
plot(angle,abs(ux_tot),'-g','LineWidth',2);
set(gca,'Fontsize',14,'FontName','Times new Roman');
xlabel('\theta (degrees) ','Fontsize',14,'FontName','Times new Roman');
ylabel('|u^{tot}_x/U_{s}|','Fontsize',14,'FontName','Times new Roman');
legend(['\eta = ',num2str(Eta),', Depth H = ', num2str(H/a),'*a']);
title('Total field displacement along ground surface');
axis([-90 270 0 1.2*max(abs(ux_tot))]);
set(gca,'XTick',(-90:30:270));
grid on
```